Published in final edited form as:
Nature. ; 482(7385): 395–399. doi:10.1038/nature10772.

Extrathymically generated regulatory T cells control mucosal Th2 inflammation

Steven Z. Josefowicz[*], **Rachel E. Niec**[*], **Hye Young Kim**, **Piper Treuting**, **Takatoshi Chinen**, **Ye Zheng**, **Dale T. Umetsu**, and **Alexander Y. Rudensky**

Abstract

A balance between pro- and anti-inflammatory mechanisms at mucosal interfaces, sites of constitutive exposure to microbes and non-microbial foreign substances, allows for efficient protection against pathogens yet prevents adverse inflammatory responses associated with allergy, asthma, and intestinal inflammation[1]. Regulatory T (Treg) cells prevent systemic and tissue-specific autoimmunity and inflammatory lesions at mucosal interfaces. These cells are generated in the thymus (tTreg cells) and in the periphery (iTreg cells) and their dual origin implies a division of labor between tTreg and iTreg cells in immune homeostasis. Here we demonstrate that a highly selective blockage in differentiation of iTreg cells did not lead to unprovoked multi-organ autoimmunity, exacerbation of induced tissue-specific autoimmune pathology (EAE), or increased pro-inflammatory Th1 and Th17 cell responses. However, iTreg cell-deficient mice spontaneously developed pronounced Th2 type pathologies at mucosal sites — in the gastrointestinal tract and lungs — with hallmarks of allergic inflammation and asthma. Furthermore, iTreg cell deficiency altered gut microbial communities. These results suggest that whereas Treg cells generated in the thymus appear sufficient for control of systemic and tissue-specific autoimmunity, extrathymic differentiation of Treg cells impacts commensal microbiota composition and serves a distinct, essential function in restraint of allergic type inflammation at mucosal interfaces.

Exquisitely balanced control mechanisms operating at mucosal sites are able to accommodate potent immune defenses against a vast array of pathogens and the need to prevent tissue damage resulting from inflammatory responses caused by commensal microorganisms and their products, food, environmental antigens, allergens, noxious substances, and toxins[1].

Prominent among multiple regulatory lymphoid and myeloid cell subsets operating at environmental interfaces are Foxp3^{+} Treg cells. Genetic deficiency in Foxp3, a key transcription factor specifying Treg cell differentiation, leads to their paucity and consequent generalized lympho- and myelo-proliferative syndrome featuring sharply augmented serum IgE levels, production of Th1, Th2, and Th17 cytokines, and widespread tissue inflammation[2]. Foxp3 can be induced in thymocytes in response to T cell receptor (TCR) and CD28 stimulation and IL-2. In addition, Foxp3 can be upregulated upon TCR stimulation of mature peripheral CD4^{+} T cells in the presence of tumor growth factor β (TGFβ) in a manner dependent on an intronic *Foxp3* enhancer CNS1[3,4,5]. Inflammatory cytokines and potent co-stimulatory signals antagonize the peripheral induction of Foxp3,

Correspondence and requests for materials should be sent to rudenska@mskcc.org.

AUTHOR CONTRIBUTIONS: S.Z.J., R.E.N., H.Y.K. performed experiments and analyzed data, with assistance from T.C. for tissue Ig ELISA experiments, and P.T. for immunohistochemistry and histopathology analysis. D.T.U., S.Z.J., R.E.N., H.Y.K, and A.Y.R designed and interpreted AHR experiments. Y.Z. generated CNS1^{-} mice. S.Z.J., R.E.N., and A.Y.R. designed experiments and wrote the paper.

The authors declare no competing financial interest.

and retinoic acid augments Foxp3 induction through mitigating inflammatory cytokine production and through cell intrinsic mechanisms[1,6,7,8]. While differing in their sites of generation, tTreg and iTreg cells are comingled in the secondary lymphoid organs and non-lymphoid tissues once mature, and their relative contributions to the total Treg cell population and their specific roles in control of various aspects of immune homeostasis and microbial colonization in normal animals has remained unexplored

Our recent investigation showed that CNS1, which contains binding sites for transcription factors (NFAT, Smad3 and RAR/RXR) downstream of three signaling pathways implicated in iTreg cell generation[4,8] (Supplementary Fig. 1), is critical for TGFβ-dependent induction of Foxp3, but has no apparent role in tTreg differentiation or maintenance of Foxp3 expression. This observation suggested that CNS1 activity represents a dedicated genetic determinant for the differentiation of iTreg cells, and its deficiency in mice provides a unique means to evaluate the function of these cells *in vivo*. Our initial characterization of CNS1^{-} mice and littermates maintained on a 129/B6 genetic background failed to reveal disease phenotypes. Since mixed genetic backgrounds frequently mask adverse phenotypes or make them highly variable, to understand iTreg function *in vivo* we backcrossed CNS1 mice onto the B6 background (Supplementary Fig. 2).

First, we sought to ascertain that on the B6 genetic background CNS1 is dispensable for tTreg cell generation but critical for generation of iTreg cells. Two recent studies established a role for TGFβ signaling in tTreg cell differentiation in neonates[9,10]. Thus, to exclude the possibility that CNS1 deficiency adversely affects generation of Foxp3^{+} T cells in the neonatal thymus we examined the Foxp3^{+} Treg cell population in heterozygous female CNS1$^{WT/-}$ mice. As Foxp3 is encoded on the X-chromosome and is subject to random X chromosome inactivation, characterization of female CNS1$^{WT/-}$ mice allows for comparison of CNS1^{-} and CNS1^{WT} Treg cells in a competitive environment. In neonatal female CNS1$^{WT/-}$ mice, CNS1^{-} cells constituted, on average, one half of the thymic Foxp3^{+} cell population (Fig. 1a). Additionally, neonatal CNS1^{-} hemizygous and control males harbored comparable numbers of Foxp3^{+} thymocytes (Supplementary Fig. 3). Therefore, tTreg differentiation is independent of CNS1. In contrast, CNS1-deficient naïve CD4 T cells showed severely impaired induction of Foxp3 in vitro (Fig. 1b). Analyses of heterozygous female CNS1$^{WT/-}$ mice and transfer of CNS1-deficient or - sufficient Treg cells into lymphopenic recipients demonstrated that the ability of Treg cells to accumulate and proliferate in various tissues was unperturbed in the absence of CNS1 (Supplementary Fig. 4). Furthermore, CNS1 deficiency did not affect suppressor activity of tTreg cells, assessed using *in vitro* suppression assays and adoptive transfers of Foxp3-deficient effector T cells with predominantly tTreg-containing Foxp3^{+} cells isolated from 4 week-old CNS1-deficient and -sufficient mice into lymphopenic recipients (Supplementary Fig. 5). Likewise, CNS1 ablation did not negatively impact maintenance of Foxp3 expression and overall function of NFAT, TGFβ, and retinoic acid signaling pathways in these cells (Supplementary Fig. 5 and data not shown). To assess how the deficiency in iTreg cell generation affects the size of the peripheral Treg cell compartment we analyzed Treg cell frequencies in various tissues throughout the lifespan of mice. CNS1^{-} mice failed to exhibit a progressive age-dependent increase in Foxp3^{+} cell frequencies observed in wild-type littermates (Fig. 1c and Supplementary Fig. 6). By 6–8 months of age CNS1^{-} mice contained markedly fewer Foxp3^{+} cells in comparison to control animals, with most prominent differences in mesenteric lymph nodes, Peyer's patches, small and large intestine lamina propria, sites known to support iTreg cell generation[11]. This trend was not the result of expression of a Foxp3-GFP fusion protein in CNS1-deficient mice, because age-matched CNS1-sufficient Foxp3-GFP and littermate control CNS1^{+} mice expressing unmodified Foxp3 protein exhibited similar age-dependent increases in Treg cell frequencies (Supplementary Fig. 6).

To assess the extent of impairment of peripheral generation of Treg cells *in vivo* we examined Foxp3 induction in antigen-specific naïve T cells upon exposure to ingested "non-self" antigen[12]. Ovalbumin (OVA)-specific OT-II$^+$ TCR-transgenic Foxp3$^-$ (GFP$^-$) Treg cells from CNS1$^-$ or *Foxp3^{GFP}* mice were transferred into CD45.1$^+$ lymphoreplete recipients followed by *ad libitum* administration of OVA in drinking water. We failed to detect Foxp3 induction in CNS1-deficient cells, whereas up to 20% of transferred OT-II T cells from control *Foxp3^{GFP}* mice induced Foxp3 upon exposure to cognate antigen in the intestinal tract (Fig. 1d and Supplementary Fig. 7). These results were in agreement with a marked impairment in Foxp3 induction in polyclonal CNS1-deficient Foxp3$^-$ T cells *in vitro*, most severe at lower, more physiologically relevant concentrations of TGFβ (Fig. 1b). Together these data indicate that iTreg cells have a stringent requirement for CNS1 for their differentiation.

Recent studies showed a limited TCR dependent clonal niche for tTreg cell differentiation and peripheral maintenance[13–15]. The sustained numerical impairment in the peripheral Treg cell populations in CNS1-deficient mice suggests that tTreg cells fail to fill the "void" in the peripheral Treg cell pool, left by iTreg cell deficiency. This observation combined with largely non-overlapping TCR repertoires of tTreg and iTreg cells suggests that iTreg and tTreg cells occupy distinct "niches"[16]. To test this notion we co-transferred CNS1-deficient (tTreg cells) or -sufficient Treg cells (iTreg + tTreg) from aged mice with CNS1-sufficient naïve Ly5.1$^+$ Foxp3$^-$ CD4$^+$ T cells into lymphopenic recipients. We observed more efficient Foxp3 induction in Ly5.1$^+$ CD4$^+$ T cells upon co-transfer with CNS1$^-$ Treg cells (tTreg cells) indicating that in lymphopenic recipients the *de novo* generation of iTreg cells is markedly more efficient in the absence of preexisting iTreg cells (Supplementary Fig. 8). These data also imply the existence of a stable iTreg cell subset in normal mice. However, the dynamics and stability of Foxp3 expression has been a controversial issue with a number of studies favoring unstable Foxp3 expression in iTreg cells[17–19]. Thus, we next employed genetic fate mapping using inducible Cre recombinase expressed in a Treg-specific manner (*Foxp3$^{EGFP\text{-}CRE\text{-}ERT2}$*) and a Rosa26-YFP recombination reporter allele (R26Y)[20] to determine if iTreg cells generated *in vivo* are able to acquire stable Foxp3 expression and, thus, have the capacity to contribute to the stable Treg cell compartment; double-sorted naïve Ly5.2$^+$ Foxp3$^-$YFP$^-$ CD4 T cells from *Foxp3$^{EGFP\text{-}CRE\text{-}ERT2}$* R26Y mice were transferred together with congenically marked Ly5.1$^-$ Foxp3$^+$ Treg cells into lymphopenic recipient mice. Foxp3 expression within the population of tagged YFP$^+$ cells generated from YFP$^-$ Foxp3$^-$ precursors was assessed four weeks after treatment of recipient mice with tamoxifen, which was administered early (one week) and late (five weeks) following cell transfer. Approximately half of the newly generated YFP-tagged iTreg cells lost Foxp3 expression, whereas "mature" iTreg cells tagged at a later time point displayed remarkable stability (>90% Foxp3$^+$ cells among YFP$^+$ cells), comparable to that of transferred peripheral Treg cells (Fig. 1e and Supplementary Fig. 9). Together these data indicate that iTreg cells have a stringent requirement for CNS1 for their differentiation, accumulate throughout life, and occupy a sizable fraction of the stable peripheral Treg cell compartment.

CNS1$^-$ mice on the B6 genetic background displayed neither early- or late-onset systemic autoimmunity nor spontaneous widespread tissue lesions or severe morbidity associated with systemic Treg cell deprivation (data not shown). However, it was possible that iTreg cell deficiency may exacerbate initial or late stages of provoked tissue-specific autoimmune pathology directed against a self-antigen. To address this question, we induced experimental autoimmune encephalomyelitis (EAE) in CNS1-deficient or littermate control mice through immunization with myelin oligodendrocyte glycoprotein (MOG) peptide. The onset, severity, and remission of disease were indistinguishable, and no detectable differences were observed in Treg cell subsets in the brain in these two groups of mice (Supplementary Fig. 10). While it will be important to evaluate the role of iTreg cells in additional models of

induced autoimmunity, these results indicate that tTreg cells are largely sufficient for control of tolerance to self-antigens and that the distinct functional role of iTreg cells might be to control inflammation at mucosal surfaces, sites of preponderant exposure to non-self substances. This notion is consistent with data indicating that tTreg cells arise from a subset of thymocytes, which exhibit TCR with an increased affinity for self-antigens yet insufficient for negative selection[10,21], whereas iTreg cells are efficiently generated upon TCR engagement with a high affinity cognate ligand under subimmunogenic conditions[22,23].

The absence of iTreg cell induction in response to oral antigen in CNS1^{-} mice suggested that the immune balance in the gastrointestinal (GI) tract might be impaired due to deficiency in gut antigen-specific iTreg cells. Indeed, while IL-17 and IFN-γ production by CD4^{+} T cells was unaffected by iTreg deficiency in CNS1^{-} mice (Supplementary Fig. 11), we observed markedly augmented production of the Th2 cytokines, IL-4, IL-5, and IL-13, by CD4^{+} T cells, especially in the mesenteric lymph nodes, Peyer's patches, and intestinal lamina propria (Fig. 2a and Supplementary Fig. 12). Furthermore, the vast majority of CD4^{+} T cells in the lamina propria of CNS1-deficient mice expressed high amounts of Gata3, a key Th2 differentiation factor. Increases in Gata3^{+} CD4^{+} T cells were observed not only in GI tract tissues in CNS1-deficient mice but also in other lymphoid tissues, albeit to a lesser extent (Fig. 2b and Supplementary Fig. 12). Consistent with the sharply augmented Th2 responses at mucosal sites, CNS1^{-} mice exhibited increased frequencies of germinal center (GC) B cells (Fas^{+}GL7^{+}) in the Peyer's patches, but not in the spleen or peripheral lymph nodes (Supplementary Fig. 13) and spontaneous increases in serum levels of IgE and IgA, but not in other Ig isotypes (Fig. c, and data not shown).

The dysregulated Th2 responses were associated with a decreased body weight (Fig. 3a and Supplementary Fig. 2) and distinct highly penetrant pathology throughout the GI tract (Fig. 3b and Supplementary Fig. 14): all CNS1^{-} (12/12) mice and none of CNS1^{+} control littermates (0/6) were affected by gastritis and plasmacytic enteritis characterized by increased frequencies of plasma cells in the intestinal lamina propria and other associated lesions such as crypt abscesses. Accordingly, serum antibodies in CNS1-deficient mice exhibited reactivity against antigens of the small and large intestine, pancreas, and chow (Supplementary Fig. 13). Notably, the pathology observed in the gastrointestinal tissue of CNS1-deficient mice was markedly diminished upon B cell depletion, but was not ameliorated by administration of IL-4 neutralizing antibody (Supplementary Fig. 15). The inflammatory features and lesions observed in CNS1-deficient mice were consistent with allergic Th2 type intestinal disease (Fig. 3).

One possible explanation for the pronounced Th2 responses and intestinal pathology associated with iTreg cell deficiency is simply a numerical decrease in Treg cells. However, we consider this possibility unlikely since graded depletion of Foxp3^{+} Treg cells in Foxp3^{DTR} mice upon administration of titrated amounts of diphtheria toxin resulting in Treg frequencies similar to those observed in CNS1^{-} mice revealed augmented Th1 and Th17, but not Th2 responses[24]. Alternatively, certain qualitative features of iTreg cells could allow them to efficiently limit Th2 inflammation in the gut. Recent studies suggested that some of the transcriptional regulators involved in a particular type of effector T cell response facilitate the ability of Treg cells to suppress those responses[25–27]. Thus, we explored the expression of Th2-associated transcription factor Gata3 in Treg cells in CNS1-deficient and -sufficient mice. In contrast to a sharp increase in Gata3 expression in effector T cells (Fig. 2b and Supplementary Fig. 12), we found its expression markedly diminished in Treg cells in CNS1-deficient mice (Fig. 3c and Supplementary Fig. 12). Notably, ablation of a conditional Gata3 allele in Treg cells leads to Treg cell dysfunction[28,29] and marked augmentation of Th2 cytokine production by CD4^{+} T cells (D. Rudra, R.N., and A.Y.R.,

manuscript in preparation). We hypothesized that increased Gata3 expression in iTreg cells reflects their activation state upon TCR ligation by high affinity ligands in the gut rather than an intrinsic feature of iTreg cells. In support of this idea, we found that both CNS1^{-} and control Treg cells stimulated *in vitro* through the TCR and IL-2 receptor exhibited similarly robust Gata3 induction (Supplementary Fig. 12). Thus, we suggest that increased Gata3 expression in iTreg cells, a likely consequence of their generation in response to high affinity TCR ligands present in the gut, endows these cells with the capacity to efficiently control spontaneous mucosal Th2 inflammation.

Certain commensal bacteria increase the frequencies of Treg cells in the gut and provide antigens recognized by a considerable proportion of iTreg TCR[1,16]. In addition to TCR ligands the gut microbial community also contributes to the local cytokine environment, which facilitates iTreg cell differentiation and maintenance in the gut[1]. These observations raise a question as to whether iTreg cells, in turn, influence composition of the commensal microbiota. To address this question we sequenced 16S ribosomal RNA coding genes from bacterial contents of stool samples isolated from CNS1-deficient and -sufficient littermates, which were housed individually for 5 weeks after weaning. Phylogenetic analysis revealed distinct gut microbial communities in CNS1^{-} mice with statistically significant enrichment of the candidate phylum TM7 and the genus Bacteroidetes alistipes (Supplementary Fig. 16), and an overall decrease in the ratio of Firmicutes to Bacteroidetes (2.60 in WT and 1.51 in KO) (Fig. 3d). Interestingly, an opposite trend in the Firmicutes/Bacteroidetes ratio was correlated with obesity[30], suggesting the possibility that alterations in energy harvest and metabolism caused by inflammation or microbe-dependent effects on energy balance, could account for the decreased weight observed in iTreg cell deficient mice. Thus, iTreg cells help maintain a “normal” microbial community in the gut likely through exerting control over Th2 mucosal inflammation.

These observations raised the question of whether the altered microbiota, rather than iTreg deficiency, was the direct cause of observed Th2 inflammation. To equalize gut microbiota, CNS1^{-} and littermate controls were treated with antibiotics (metronidazole and ciprofloxacin) for 4 weeks. Despite indistinguishable microbial communities, antibiotic treatment did not lead to a decrease in Gata3 expression or Th2 cytokine production by effector T cells in CNS1-deficient mice and characteristic histopathologic features were maintained (Supplementary Fig. 17). Furthermore, iTreg cell sufficient germ-free mice colonized with CNS1^{-} or control microbiota exhibited a similar spectrum of Th1, Th2, and Th17 cytokine production and eventual normalization of microbiota (Supplementary Fig. 18 and data not shown). These results suggest that iTreg deficiency results in immune dysregulation and Th2 inflammation in the gut with subsequent perturbation of the microbial community.

According to the notion of specialized iTreg cell function in suppression of Th2 responses at mucosal sites, one would expect to observe Th2 type pathology in the lungs of CNS1-deficient mice, despite an only modest ~20–25% decrease in Treg cell numbers in this tissue compared to littermate controls (Fig. 1c). Indeed, we discovered that CNS1^{-} mice suffer from spontaneous Th2-type airway inflammation (Fig. 4 and Supplementary Fig. 19). The lungs of CNS1^{-} mice were characterized by increased infiltration by lymphocytes, plasma cells, macrophages, and moderate neutrophil infiltration (Fig. 4a and g). The consistent features of the chronic inflammatory airway disease observed in CNS1^{-} mice include lymphocytic infiltration, narrowed airway lumen (Fig. 4a), increased goblet cells and mucus production (Fig. 4a and b), smooth muscle hyperplasia, and fibrosis (Fig. 4c). Notably, 9/12 CNS1^{-} and 0/6 CNS1^{+} mice developed acidophilic macrophage pneumonia (AMP) with characteristic increases in acidophilic macrophages and both intracellular and extracellular Chitinase 3-like 3 crystals (C3l3, formerly Ym1) analogous to Charcott-Lyden crystals

found in asthmatic patients (Fig. 4a and e). In addition, prominent presence of alternatively activated macrophages in the lungs of CNS1-deficient mice was confirmed by morphology and expression of Arginase 1 in addition to C3l3 (Fig. 4d and Supplementary Fig. 20). Furthermore, both young (6–8 week old) and aged (20 week old) unimmunized CNS1^{-} mice exhibited airway hyper-responsiveness accompanied by AMP, perivascular, peribronchiolar, and intramucosal inflammation, bronchial epithelial hyperplasia, and airway narrowing (Fig. 4f and Supplementary Fig. 21). These spontaneous lesions are especially striking considering the Th2-resistant, Th1-prone C57BL/6 genetic background of CNS1-deficient mice. The lung pathology in CNS1^{-} mice reflects the hallmark features of chronic allergic inflammation and asthma.

Our results demonstrate that Treg cells of thymic and extrathymic origin have distinct mechanistic requirements for differentiation and exert specialized functions in immune homeostasis. The restriction of lesions to mucosal tissues in iTreg deficient mice implies that under steady state conditions Treg cells generated in the thymus are largely sufficient for control of most immune responses to self-antigens. These findings suggest that in normal animals, Treg cells generated extrathymically in a CNS1-dependent manner play a non-redundant role in control of mucosal allergic Th2 inflammation and asthma.

METHODS

Mice

The generation of the following mouse strains has been previously described: CNS1^{-} (*Foxp3*$^{\Delta CNS1}$), *Foxp3*^{GFP}, and *Foxp3*$^{eGFP\text{-}Cre\text{-}ERT2}$ R26Y[5,20]. *Rag1*$^{-}$ mice were purchased from The Jackson laboratory (ME), and CD45.1 B6 and *Tcrb/Tcrd*$^{-/-}$ mice, along with above strains were maintained in the Sloan Kettering Institute Research Laboratories animal facility in accordance with institutional regulations. Mice were euthanized by CO_2 asphyxiation. EAE was induced and scored as previously described[31]. For antibiotic treatment, CNS1-deficient and sufficient mice were treated with 1 g/L metronidazole (Sigma-Aldrich) and 0.2 g/L ciprofloxacin (ENZO Life Sciences International) dissolved in drinking water for 4 weeks. Mouse anti-CD20[8] (MB20-11, kindly provided by Dr. Thomas Tedder) and anti-IL-4 (11b.11, NCI-Frederick) were administered weekly intraperitoneal injections of 50 μg or 5 μg, respectively, for 3 weeks.

Cell isolation, transfer and FACS staining

For *in vitro* and *in vivo* transfer experiments, CD4^{+} T cells were pre-enriched using mouse CD4 Dynabeads (L3T4, Invitrogen) and FACS sorted on an LSR-II (BD Biosciences). Intracellular staining for IL-4 utilized Cytofix/Cytoperm following treatment with Golgi-Stop (BD Biosciences), and staining for other cytokines (following treatment with Golgi-Plug, BD Biosciences) and Foxp3 and Gata3 utilized the Foxp3 staining kit (eBiosciences).

In vitro assays

In vitro induction assays were performed with 5×10^{4} Foxp3-GFP^{-} CD4^{+} T cells and 5 ug/mL of anti-CD3 and anti-CD28 antibody, 100U/mL IL-2, in 96 well, flat-bottom plates. For *in vitro* suppression assays, 4 × 10^{4} CD4^{+}Foxp3^{-}CD62L^{high} naive T cells FACS purified from WT mice were cultured with graded numbers of CD4^{+}Foxp3^{+} Treg cells FACS purified from *Foxp3*$^{\Delta CNS1}$ or *Foxp3*^{gfp} mice in the presence of 10^{5} irradiated T cell–depleted splenocytes and 1 μg/ml anti-CD3 antibody in a 96-well round-bottom plate for 80 h. Cell proliferation was assessed by [^{3}H]thymidine incorporation during the final 8 h of culture.

Histology and Immunohistochemistry

Necropsies were performed and sections of pancreas, stomach, heart, lungs, kidney, external ear and haired skin were fixed in 10% phosphate-buffered formalin. Tissues were processed routinely for staining with hematoxylin and eosin (H&E), periodic acid Schiff with Alcian blue or Masson Trichrome if indicated. Slides were examined by a board-certified veterinary pathologist blinded to genotypes. Morphological diagnoses were applied for all tissues. Immunohistochemical staining was performed by the University of Washington Histology and Imaging Core using standard protocols with a Leica Bond Automated Immunostainer. Primary antibodies: goat anti mouse Chitinase 3 like 3/ECF-L (YM1),(R&D systems, Cat No. AF2446, Lot No. UNU01), (0.2 μg/mL); rabbit polyclonal anti iNOS/NOS II, NT (Millipore, Cat No. 06-573) (1 μg/mL); rabbit polyclonal anti arginase 1 (H-52) (Santa Cruz, Cat No. sc-20150, Lot No. K0807) (0.2 μg/mL). Isotype controls were used at the same concentration as the primary antibody with all antibodies run with Lecia Bond reagents and Bond Polymer Refine (DAB) detection with hematoxylin counter stain.

Histology inflammation scoring

0. None; **1.** Focal or multifocal mild perivascular accumulations with minimal extension into surrounding adventia or parenchyma; **2.** Multifocal mild or focal moderate perivascular accumulations with mild extension into surrounding parenchyma or mild to moderate parenchymal accumulations; **3.** Grade 2 plus mild inflammation-associated parenchymal lesions such as loss or degeneration of cells; **4.** Grade 2 plus moderate to severe inflammation-associated parenchymal lesions. Inflammation in the gastrointestinal tract was scored as described previously[32].

Airway hyperresponsiveness measurements

For measurement of AHR, mice were anesthetized with pentobarbitol (7.5–10 mg/mice) and AHR was assessed by invasive measurement of airway resistance using modified version of a described method (Buxco Electronics). Mice were ventilated at a tidal volume of 0.2 ml with the use of a ventilator (Harvard Apparatus, Holliston, MA) and frequency was set around 150 Hz. Baseline pulmonary mechanics and responses to ventilated saline (0.9% NaCl) were measured, and lung resistance (R_L) was measured in response to increasing doses (0.125 to 40 mg/ml) of acetyl-b-methylcholine chloride (methacholine; MCh) (Sigma-Aldrich, St. Louis, MO). The 3 values of R_L obtained after each dose of methacholine were averaged to obtain the final values for each dose. Results are expressed as percentage of increase of saline-baseline. Following measurement of AHR, mouse tracheas were cannulated and the lungs were lavaged twice with 1 ml of PBS 2% FCS and the fluids were pooled. Cells in the lavage fluid were counted using a hemocytometer, and BAL cell differential counts were determined on slide preparations stained with DiffQuik. At least 200 cells were differentiated on stained slides by light microscopy using conventional morphological criteria. For some experiments, BAL for each mouse or grouped BAL was stained and analyzed by flow cytometry.

Stool sample collection

Fresh stool samples were induced directly into sterile collection tubes from live CNS1^{-} and control mice and snap frozen before preparation of material for sequencing (see below).

DNA extraction, PCR amplification and sequencing, Sequence processing and analysis

DNA extraction—DNA extraction was performed on each fecal specimen using phenol-chloroform extraction with mechanical disruption based on a previously described protocol[33] Briefly, an aliquot (~500 mg) of each sample was suspended in a solution containing 500 μl of extraction buffer (200 mM Tris, pH 8.0; 200 mM NaCl; and 20 mM

EDTA), 210 μl of 20% SDS, 500 μl of phenol/chloroform/isoamyl alcohol (25:24:1), and 500 μl of 0.1-mm-diameter zirconia/silica beads (BioSpec Products). Microbial cells were lysed by mechanical disruption with a bead beater (BioSpec Products) for 2 minutes, after which 2 rounds of phenol/chloroform/isoamyl alcohol extraction were performed. DNA was precipitated with ethanol and resuspended in 50 μl of nuclease-free water. DNA was subjected to additional purification with the QIAamp DNA Mini Kit (Qiagen).

PCR amplification and sequencing—For each sample, 3 replicate 25 μl PCR amplifications were performed, each containing 5 ng of purified DNA, 0.2 mM dNTPs, 1.5 mM MgCl2, 1.25 U Platinum Taq DNA polymerase, 2.5 μl of 10× PCR buffer, and 0.2 μM each of broad-range bacterial forward and reverse primers as described previously[34], flanking the V1–V3 variable region. The primers were modified to include adaptor sequences required for 454 sequencing, with the addition of a unique 6 – 8 base barcode in the reverse primer. The forward primer (5'-CCTATCCCCTGTGTGCCTTGGCAGTCTC*AGAGTTTGATCCTGGCTCAG*-3') consisted of the 454 Lib-L primer B (underline) and the broad-range universal bacterial primer 8F (italics); the reverse primer (5′-CCATCTCATCCCTGCGTGTCTCCGACTCAGNNNNNNN*ATTACCGCGGCTGCTGG*-3′) consisted of the 454 Lib-L primer A, barcode (NNNNNNN), and the broad-range primer 534R (italics). The cycling conditions were: 94 °C for 3 min, then 25 cycles of 94 °C for 30 sec, 56 °C for 30 sec, and 72 °C for 1 min. The three replicate PCR products were pooled and subsequently purified using the Qiaquick PCR Purification Kit (Qiagen). The purified PCR products were sequenced unidirectionally on a 454 GS FLX Titanium pyrosequencing platform following the Roche 454 recommended procedures.

Sequence processing and analysis—Sequences were converted to standard FASTA format using Vendor 454 software. Sequences shorter than 200 bp, containing undetermined bases or homopolymer stretches longer than 8 bp, or failing to align with the V1 – V3 region were excluded from the analysis. Using the 454 base quality scores, which range from 0 – 40 (0 being an ambiguous base), sequences were trimmed using a sliding-window technique, such that the minimum average quality score over a window of 50 bases never dropped below 35. Sequences were trimmed from the 3'-end until this criterion was met. Sequences were aligned to the V1 – V3 region of the 16S gene, using as template the SILVA reference alignment[35] and the Needleman-Wunsch algorithm with default scoring options. Potentially chimeric sequences were removed using the chimera uchime program[36]. Sequences were grouped into operational taxonomic units (OTUs) using the average neighbor algorithm. Sequences with distance-based similarity of 97% or greater were assigned to the same OTU. For each fecal sample, OTU-based microbial diversity was estimated by calculating the Shannon diversity index[37]. Phylogenetic classification to genus level was performed for each sequence, using the Bayesian classifier algorithm described by Wang and colleagues, using a database of known 16S sequences generated by the Ribosomal Database Project (RDP)[38]. For each experiment, data were analyzed on each taxon level individually. The count data was rescaled using DESeq R package[39]. Bacteria with less than 10 mean count in both conditions were removed from further analysis and bacteria with statistically significant differences between two conditions (e.g. WT and KO), were determined using binomial test (from DESeq package). Bacteria with fold-change greater than two and FDR = 0.05 were declared significant.

Supplementary Material

Refer to Web version on PubMed Central for supplementary material.

Acknowledgments

We thank T. Tedder (Duke University) for depleting CD20 antibody, R. Tudor (University of Colorado) for assistance interpreting lung pathology, P. DeRoos for assistance with Ig ELISA assays, Brian Johnson for immunohistochemical expertise, Y. Chen for assistance with airway measurements, and E. Pamer, L. Lipuma, A. Gobourne and R. Khanin for help with analysis of intestinal microbiota. This work was supported by NIH MSTP grant GM07739 and NINDS grant 1F31NS073203-01 (R.E.N.) and NIH grant R37 AI034206 (A.Y.R.). A.Y.R is an investigator with the Howard Hughes Medical Institute.

REFERENCES

1. Maloy KJ, Powrie F. Intestinal homeostasis and its breakdown in inflammatory bowel disease. Nature. 474(7351):298–306. [PubMed: 21677746]
2. Sakaguchi S, Yamaguchi T, Nomura T, Ono M. Regulatory T cells and immune tolerance. Cell. 2008; 133(5):775–787. [PubMed: 18510923]
3. Chen W, et al. Conversion of peripheral CD4+CD25− naive T cells to CD4+CD25+ regulatory T cells by TGF-beta induction of transcription factor Foxp3. J Exp Med. 2003; 198(12):1875–1886. [PubMed: 14676299]
4. Tone Y, et al. Smad3 and NFAT cooperate to induce Foxp3 expression through its enhancer. Nat Immunol. 2008; 9(2):194–202. [PubMed: 18157133]
5. Zheng Y, et al. Role of conserved non-coding DNA elements in the Foxp3 gene in regulatory T-cell fate. Nature. 463(7282):808–812. [PubMed: 20072126]
6. Hill JA, et al. Retinoic acid enhances Foxp3 induction indirectly by relieving inhibition from CD4+CD44hi Cells. Immunity. 2008; 29(5):758–770. [PubMed: 19006694]
7. Nolting J, et al. Retinoic acid can enhance conversion of naive into regulatory T cells independently of secreted cytokines. J Exp Med. 2009; 206(10):2131–2139. [PubMed: 19737861]
8. Xu L, et al. Positive and negative transcriptional regulation of the Foxp3 gene is mediated by access and binding of the Smad3 protein to enhancer I. Immunity. 33(3):313–325. [PubMed: 20870174]
9. Liu Y, et al. A critical function for TGF-beta signaling in the development of natural CD4+CD25+Foxp3+ regulatory T cells. Nat Immunol. 2008; 9(6):632–640. [PubMed: 18438410]
10. Ouyang W, Beckett O, Ma Q, Li MO. Transforming growth factor-beta signaling curbs thymic negative selection promoting regulatory T cell development. Immunity. 32(5):642–653. [PubMed: 20471291]
11. Curotto de Lafaille MA, Lafaille JJ. Natural and adaptive foxp3+ regulatory T cells: more of the same or a division of labor? Immunity. 2009; 30(5):626–635. [PubMed: 19464985]
12. Mucida D, et al. Oral tolerance in the absence of naturally occurring Tregs. J Clin Invest. 2005; 115(7):1923–1933. [PubMed: 15937545]
13. Bautista JL, et al. Intraclonal competition limits the fate determination of regulatory T cells in the thymus. Nat Immunol. 2009; 10(6):610–617. [PubMed: 19430476]
14. Leung MW, Shen S, Lafaille JJ. TCR-dependent differentiation of thymic Foxp3+ cells is limited to small clonal sizes. J Exp Med. 2009; 206(10):2121–2130. [PubMed: 19737865]
15. Moran AE, et al. T cell receptor signal strength in Treg and iNKT cell development demonstrated by a novel fluorescent reporter mouse. J Exp Med. 208(6):1279–1289. [PubMed: 21606508]
16. Lathrop SK, et al. Peripheral education of the immune system by colonic commensal microbiota. Nature. 478(7368):250–254. [PubMed: 21937990]
17. Komatsu N, et al. Heterogeneity of natural Foxp3+ T cells: a committed regulatory T-cell lineage and an uncommitted minor population retaining plasticity. Proc Natl Acad Sci U S A. 2009; 106(6):1903–1908. [PubMed: 19174509]
18. Hori S. Regulatory T cell plasticity: beyond the controversies. Trends Immunol. 32(7):295–300. [PubMed: 21636323]
19. Zhou X, et al. Instability of the transcription factor Foxp3 leads to the generation of pathogenic memory T cells in vivo. Nat Immunol. 2009; 10(9):1000–1007. [PubMed: 19633673]
20. Rubtsov YP, et al. Stability of the regulatory T cell lineage in vivo. Science. 329(5999):1667–1671. [PubMed: 20929851]

21. Josefowicz SZ, Rudensky A. Control of regulatory T cell lineage commitment and maintenance. Immunity. 2009; 30(5):616–625. [PubMed: 19464984]
22. Gottschalk RA, Corse E, Allison JP. TCR ligand density and affinity determine peripheral induction of Foxp3 in vivo. J Exp Med. 207(8):1701–1711. [PubMed: 20660617]
23. Kretschmer K, et al. Inducing and expanding regulatory T cell populations by foreign antigen. Nat Immunol. 2005; 6(12):1219–1227. [PubMed: 16244650]
24. Tian L, et al. Foxp3 regulatory T cells exert asymmetric control over murine helper responses by inducing Th2 cell apoptosis. Blood. 2011; 118(7):1845–1853. [PubMed: 21715314]
25. Chaudhry A, et al. CD4+ regulatory T cells control TH17 responses in a Stat3-dependent manner. Science. 2009; 326(5955):986–991. [PubMed: 19797626]
26. Koch MA, et al. The transcription factor T-bet controls regulatory T cell homeostasis and function during type 1 inflammation. Nat Immunol. 2009; 10(6):595–602. [PubMed: 19412181]
27. Zheng Y, et al. Regulatory T-cell suppressor program co-opts transcription factor IRF4 to control T(H)2 responses. Nature. 2009; 458(7236):351–356. [PubMed: 19182775]
28. Wang Y, Su MA, Wan YY. An Essential Role of the Transcription Factor GATA-3 for the Function of Regulatory T Cells. Immunity. 35(3):337–348. [PubMed: 21924928]
29. Wohlfert EA, et al. GATA3 controls Foxp3+ regulatory T cell fate during inflammation in mice. J Clin Invest. 2011
30. Turnbaugh PJ, et al. An obesity-associated gut microbiome with increased capacity for energy harvest. Nature. 2006; 444(7122):1027–1031. [PubMed: 17183312]

Supplemental References

31. Stromnes IM, Goverman JM. Active induction of experimental allergic encephalomyelitis. Nat Protoc. 2006; 1(4):1810–1819. [PubMed: 17487163]
32. Burich A, et al. Helicobacter-induced inflammatory bowel disease in IL-10- and T cell-deficient mice. Am. J. Physiol. Gastrointest. Liver Physiol. 2001; 281:G764–G778. [PubMed: 11518689]
33. Ubeda C, et al. Vancomycin-resistant Enterococcus domination of intestinal microbiota is enabled by antibiotic treatment in mice and precedes bloodstream invasion in humans. J Clin Invest. 2010; 120:4332–4341. [PubMed: 21099116]
34. Nossa C, et al. Design of 16S rRNA gene primers for 454 pyrosequencing of the human foregut microbiome. World J Gastroenterol. 2010; 16:4135–4144. [PubMed: 20806429]
35. Schloss PD, et al. Introducing mothur: open-source, platform-independent, community-supported software for describing and comparing microbial communities. Appl Environ Microbiol. 2009; 75:7537–7541. [PubMed: 19801464]
36. Edgar RC, et al. UCHIME improves sensitivity and speed of chimera detection. Bioinformatics. 2011; 27:2194–2200. [PubMed: 21700674]
37. Magurran, AE. Measuring biological diversity. Malden, Ma: Blackwell Pub.; 2004.
38. Wang Q, et al. Naive Bayesian classifier for rapid assignment of rRNA sequences into the new bacterial taxonomy. Appl Environ Microbiol. 2007; 73:5261–5267. [PubMed: 17586664]
39. Anders S, Huber W. Differential expression analysis for sequence count data. Genome Biology. 2010; 11:R106. [PubMed: 20979621]

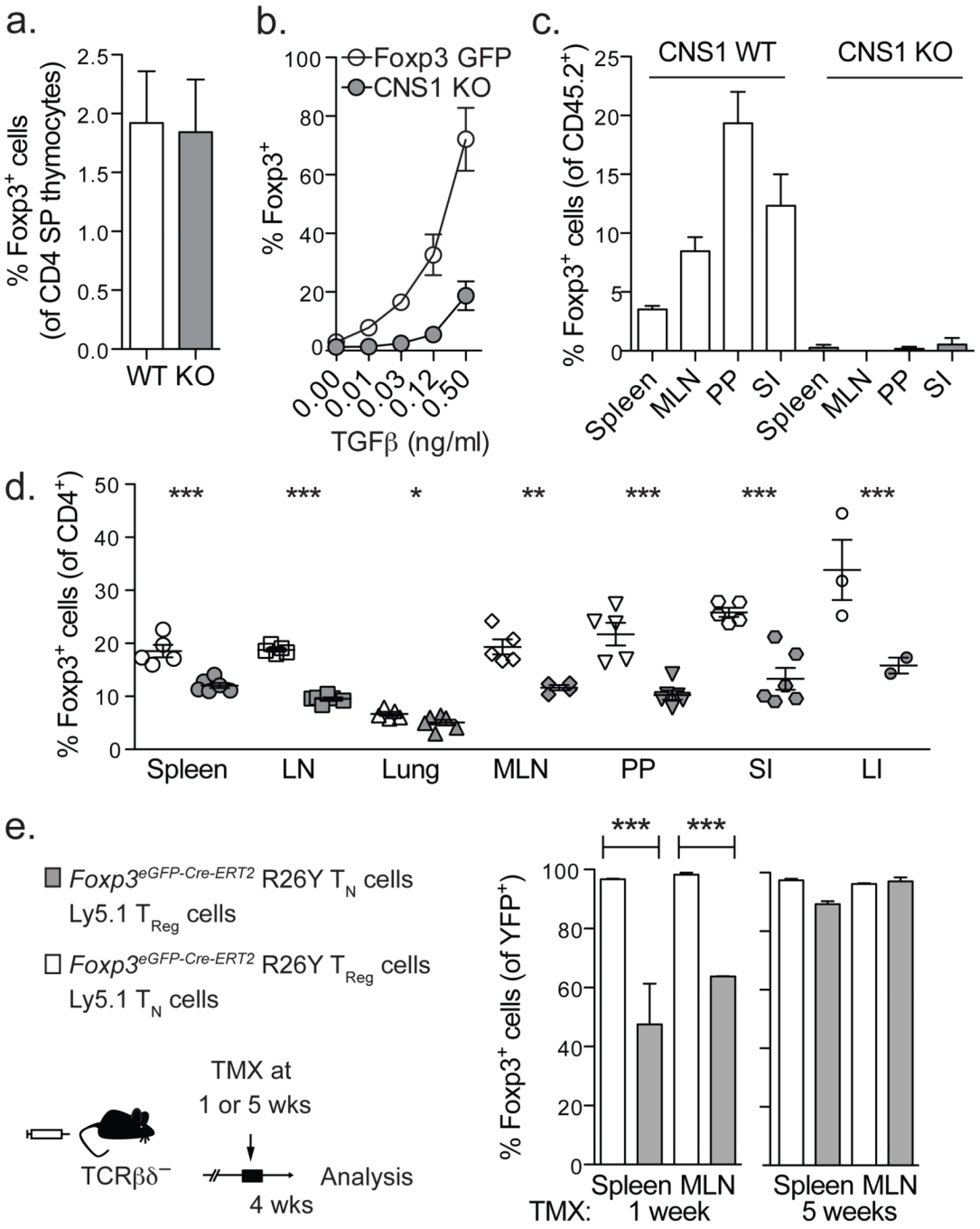

Figure 1. Impaired iTreg cell generation and altered composition of the peripheral Treg cell population in CNS1-deficient mice

a, Relative contribution of CNS1-deficient (GFP^+) and -sufficient (GFP^-) cells to the $Foxp3^+$ thymocyte subset in 4-day-old $CNS1^{+/-}$ female mice.

b, Induction of Foxp3 in $Foxp3^-$ T_N cells FACS sorted from $CNS1^-$ or *Foxp3*^{GFP} mice stimulated *in vitro* with TGFβ, IL-2, anti-CD3 and anti-CD28.

c, Percent $Foxp3^+$ cells in the spleen, lymph node (LN), mesenteric lymph nodes (MLN), Peyer's patches (PP) and cells from the small and large intestine lamina propria (SI and LI) of 6–9 month old $CNS1^-$ or control mice.

d, Percent of transferred CNS1^{-} or CNS1^{+} CD25^{-}CD44^{low}CD45.2^{+}OTII^{+} cells that induced Foxp3 following administration of OVA in water for 6 days.
e, Stability of Foxp3 expression in iTreg cells. FACS sorted GFP^{+} or GFP^{-} cells from *Foxp3*$^{eGFP\text{-}Cre\text{-}ERT2}$ mice were transferred with GFP^{-} or GFP^{+} cells, respectively, from Ly5.1 *Foxp3*^{GFP} mice into TCRβδ-deficient recipients. Mice received tamoxifen at 1 (left) or 5 weeks (right) post transfer and stability of Foxp3 expression among YFP-labeled cells was assessed after 4 weeks. All data are representative of two or more independent experiments with n ≥ 3. Error bars represent SD; *, **, and *** indicate p <0.05, 0.01 and 0.001, respectively, as calculated by students' T-test.

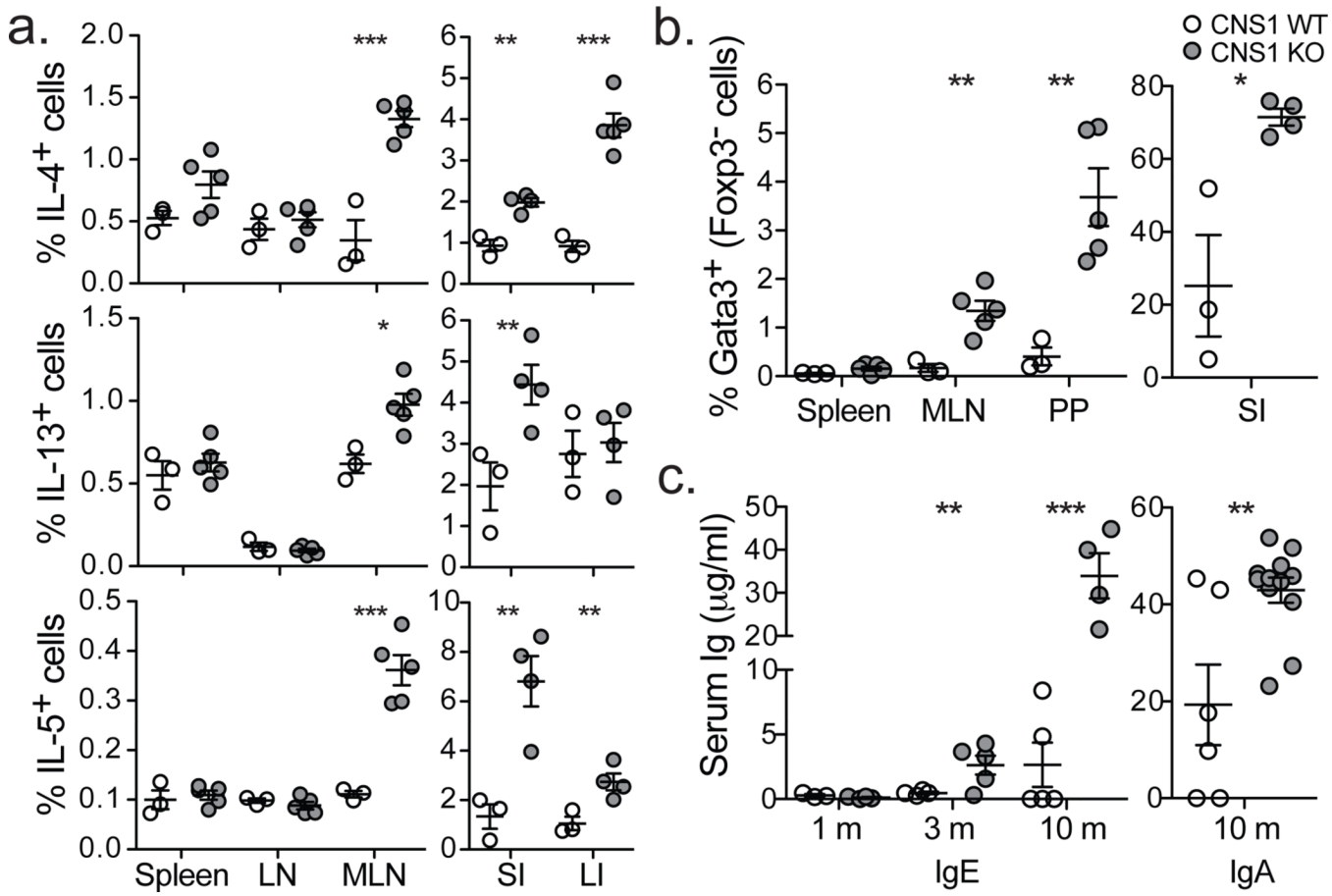

Figure 2. Paucity of iTreg cells results in Th2 inflammation in the gastrointestinal tract

a, Percent of $CD4^+$ cells producing IL-4, IL-13 and IL-5 in 3-month-old mice.

b, Percent of $Foxp3^-$ $CD4^+$ cells that were Gata3+ in 3-month old mice.

c, Concentration of IgE and IgA in serum, determined by enzyme linked immunosorbent assay (ELISA).

All data are representative of three or more independent experiments with ≥ 3 mice per group. Error bars represent SD; *, **, and *** indicate $p < 0.05$, 0.01 and 0.001, respectively, as calculated by students' T-test.

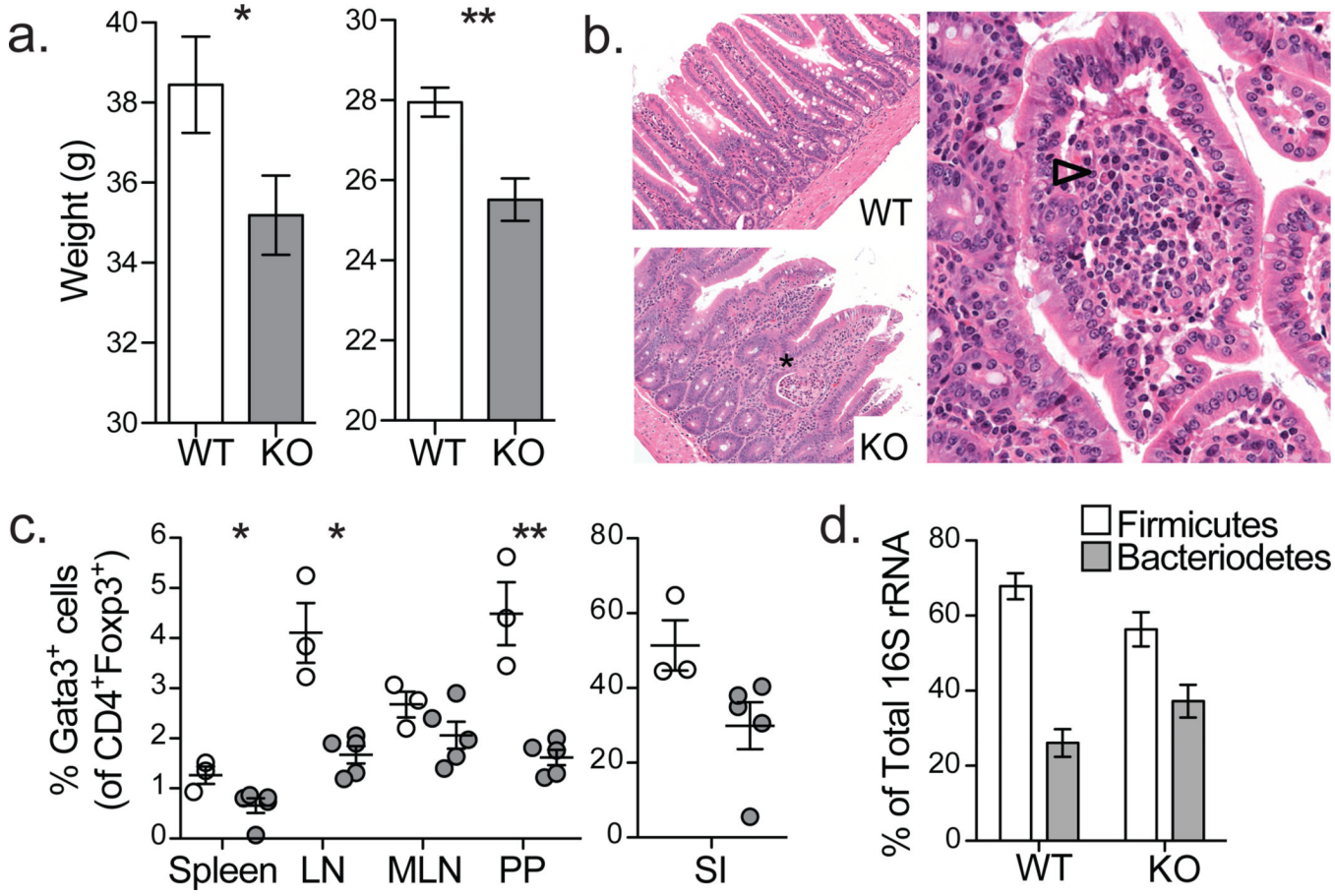

Figure 3. iTreg cells deficiency leads to Th2 type gastrointestinal pathology and altered microbial communities

a, Body weights of 9–12 (left) or 2.5-month-old individually housed (right) CNS1^{-} and littermate control mice (n ≥ 12).

b, Plasmacytic enteritis (arrowhead) in CNS1-deficient mice revealed by H&E staining of small intestine from 9–12-month-old CNS1^{-} (bottom and right) and littermate control mice (top). An early crypt abscess is indicated (asterisk). Data represent ≥ 20 mice.

c, Percent of Foxp3^{+} CD4^{+} cells expressing Gata3^{+} in 3-month old mice.

d, Percent of total 16S rRNA gene sequences of the Firmicutes and Bacteroidetes phyla in stool from individually housed CNS1^{-} (n=9) and WT (n=6) littermate mice. Mean values $^{+}$/$^{-}$ SEM are shown.

All data are representative of three or more independent experiments with ≥ 3 mice per group. Error bars represent SD; *, **, and *** indicate p <0.05, 0.01 and 0.001, respectively, as calculated by students' T-test. Scale bars = 150 um.

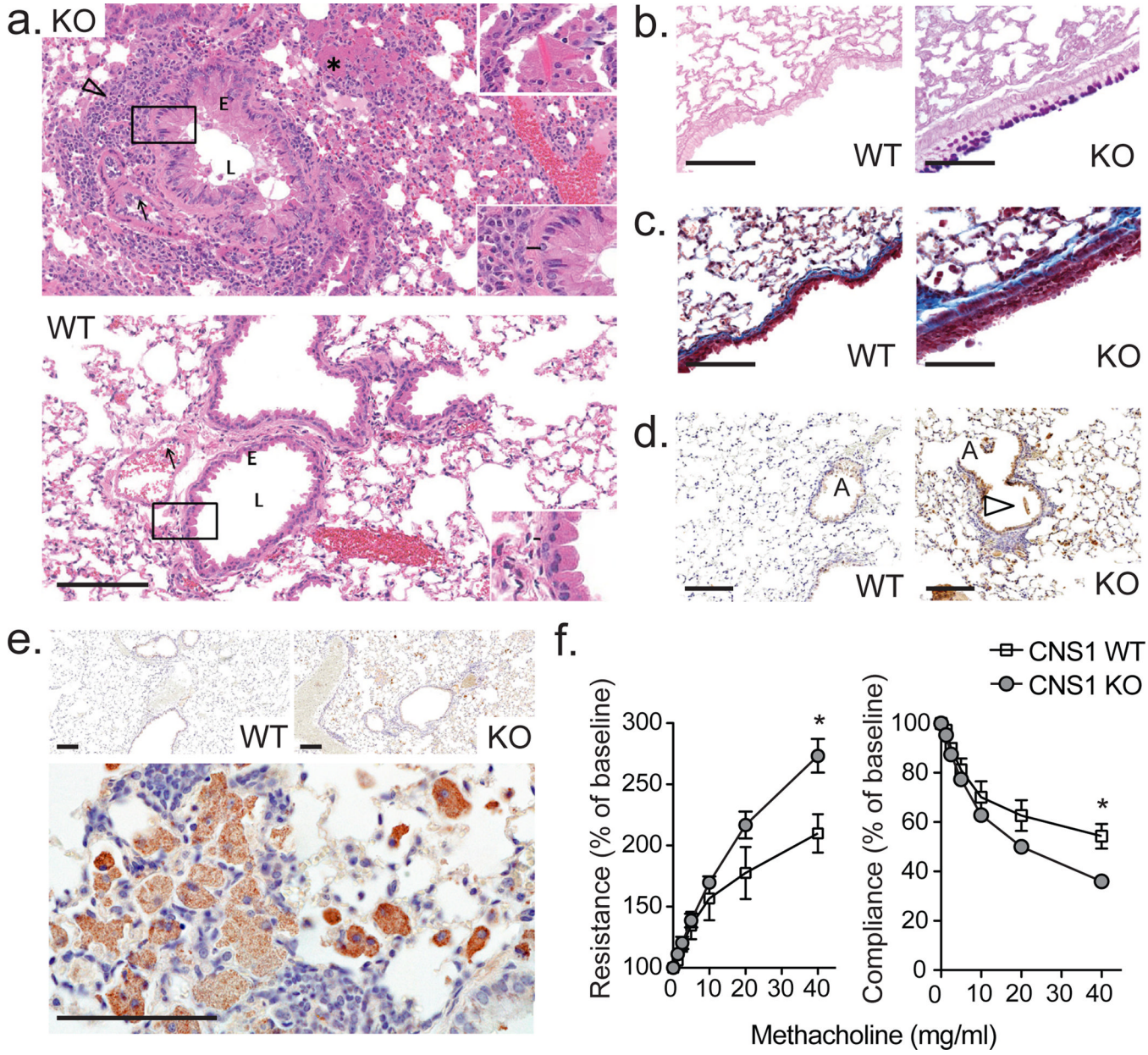

Figure 4. Unprovoked asthma-like airway pathology in CNS1-deficient mice

a, Representative H&E-stained lung section form CNS1^{-} (top) and WT (bottom) mice. The CNS1^{-} lung has marked peribronchiolar inflammation (arrowhead). The reduced lumen (L) contains mucus produced by the hyperplastic respiratory epithelium (E) Arrows indicate reactive (top) and normal (bottom) endothelium. Bottom right hand corner insets are higher magnification of boxed regions and bar indicates smooth muscle thickness. Top right inset (KO) demonstrates eosinophilic crystals. Asterisk marks acidophilic macrophages.

b, PAS/AB staining highlighting mucus-producing goblet cells (dark blue-purple)

c, Trichrome staining illustrating lung fibrosis (blue staining).

d, Arginase-1 staining of lungs from CNS1^{-} and WT mice. “A” indicates airway; an acidophilic crystal is marked by the arrowhead.

e, Chitinase 3-like 3 (C3l3) staining of lungs from CNS1^{-} and WT mice at 10× amplification (top) and 60× magnification of lungs from CNS1^{-} mice demonstrating robust C3l3 expression within acidophilic macrophages (bottom).
f, Lung resistance (left) and compliance (right) of CNS1^{-} and wild type littermate control mice after exposure to methacholine.
Data representative of 2 independent experiments with ≥ 4 mice per group. Error bars represent SD; *, **, and *** indicate $p < 0.05$, 0.01 and 0.001, respectively, as calculated by students' T-test. Scale bars = 100 um.